Translation inhibition and resource balance in the TX-TL cell-free gene expression system

Vijayalakshmi H. Nagaraj[1], James M. Greene[2], Anirvan M. Sengupta[3,*], and Eduardo D. Sontag[4,*]

[1]Department of Physics and Astronomy, Center for Quantitative Biology (CQB), Rutgers University, Piscataway, NJ, USA, [2]Department of Mathematics and CQB, Rutgers University, Piscataway, NJ, USA, [3]Department of Physics and Astronomy and CQB, Rutgers University, Piscataway, NJ, USA and [4]Department of Mathematics and CQB, Rutgers University, Piscataway, NJ, USA

*Corresponding author: E-mail: anirvans.physics@gmail.com; eduardo.sontag@gmail.com

Abstract

Quantifying the effect of vital resources on transcription (TX) and translation (TL) helps to understand the degree to which the concentration of each resource must be regulated for achieving homeostasis. Utilizing the synthetic TX-TL system, we study the impact of nucleotide triphosphates (NTPs) and magnesium (Mg^{2+}) on gene expression. Recent observations of the counter-intuitive phenomenon of suppression of gene expression at high NTP concentrations have led to the speculation that such suppression is due to the consumption of resources by TX, hence leaving fewer resources for TL. In this work, we investigate an alternative hypothesis: direct suppression of the TL rate via stoichiometric mismatch in necessary reagents. We observe NTP-dependent suppression even in the early phase of gene expression, contradicting the resource-limitation argument. To further decouple the contributions of TX and TL, we performed gene expression experiments with purified messenger RNA (mRNA). Simultaneously monitoring mRNA and protein abundances allowed us to extract a time-dependent translation rate. Measuring TL rates for different Mg^{2+} and NTP concentrations, we observe a complex resource dependence. We demonstrate that TL is the rate-limiting process that is directly inhibited by high NTP concentrations. Additional Mg^{2+} can partially reverse this inhibition. In several experiments, we observe two maxima of the TL rate viewed as a function of both Mg^{2+} and NTP concentration, which can be explained in terms of an NTP-independent effect on the ribosome complex and an NTP-Mg^{2+} titration effect. The non-trivial compensatory effects of abundance of different vital resources signal the presence of complex regulatory mechanisms to achieve optimal gene expression.

Key words: cell-free systems; *in vitro* synthetic biology; RNA aptamer; translation rate; homeostasis.

1. Introduction

Escherichia coli cell-free transcription–translation (TX-TL) systems (1–7) provide promising tools for characterizing genetic networks in a minimally complex environment and have been proposed as a technique for large-scale industrial synthesis of bioproducts ranging from synthetic fuels to drugs (8). As a design tool, this technique allows biological engineers to explore genetic circuits in an analogous way to that in which electrical engineers use breadboards to understand electronic circuits. From a fundamental biology standpoint, the greater control provided over experimental conditions allows one to obtain a quantitative understanding of gene expression dynamics.

The experimental conditions in the TX-TL expression system must be precisely calibrated for optimal expression. Not

only do various ion concentrations need to be accurately prescribed but even resources such as nucleotide triphosphates (NTPs) have to be optimized carefully for significant expression to occur. Our understanding of the resource requirements of gene expression is challenged by the observation that gene expression decreases with NTP concentration, once NTP is increased beyond a certain threshold (9). This phenomenon is unexpected, because higher amounts of NTPs imply a greater source of energy available for TX and TL. Siegal-Gaskins *et al.* (9) speculate that increased NTP levels enhance transcriptional activity and thus exhaust most of the present NTPs. As a result, very little resources remain for TL to proceed, explaining the reduction of gene expression. In our investigations, we contrast this hypothesis with a simpler explanation involving a direct suppression of gene expression, specifically that of the translation rate as a function of the overabundance of certain reagents.

In our system, which has no significant protein degradation mechanism, conversion of adenosine triphosphate (ATP) to adenosine diphosphate (ADP) and the subsequent rise of ADP/ATP ratio (10) slow down protein production rates. A few hours into the experiment, this slowdown causes protein levels to saturate. Analyzing the gene expression profile thus requires us to be cognizant of the temporal dependence of TX and, particularly, TL rates. We have developed methods of extracting such time-dependent rates.

One could reasonably believe that at times prior to saturation, resource limitation is peripheral to the underlying dynamics of gene expression. Therefore, monitoring the protein and RNA levels at early times as a function of NTP and other reagents allows us to differentiate protein level suppression at high NTP concentrations. In general, we will use this experimental strategy to explore the landscape of resource dependence in the TX-TL system.

2. Materials and methods

2.1 Cell-free reaction conditions

Crude extract was prepared from BL21-Rosetta 2 strain, following the protocol of Sun *et al.* (6). Basic cell-free reactions consist of a crude cell extract from *E. coli* (which contains endogenous TX-TL machinery, mRNA and protein degradation enzymes plus all the soluble proteins), buffer and DNA. The amino acid mix was prepared following the protocol from (11). All the experiments shown here were performed using the same batch of extract preparation to avoid variation between different batches. Reactions were carried out in a 10-µl volume using 1–2 nM plasmid, 10–20 µM malachite green (MG) to simultaneously monitor the RNA production. The reaction temperature was set to 29°C. Experiments were run for 14–20 h with readings taken every 20 min, so that green fluorescent protein (GFP) and RNA expression dynamics could be monitored over a long period of time.

2.2 Monitoring RNA production

Messenger RNA production was monitored using a plasmid provided by Dr. Murray's lab, which consists of a 35-bp (MGapt) aptamer sequence incorporated in the 3′ untranslated region of the fluorescent protein reporter gene, 15 bases downstream of the stop codon and capable of binding the dye MG and produces fluorescence signal that can be measured at 650 nm wavelength. Fluorescence measurements were made in a total of six wells for each condition in a Biotek plate reader at 20-min

intervals using excitation/emission wavelengths set at 610/650 nm (MGapt) and 485/525 nm (deGFP). Error bars indicate standard error over six replicates. The reported protein production at each time point represents a 20-min time interval.

2.3 Plasmids and bacterial strains

Plasmids used in our study are pBEST-Pr-GFP-MG (Addgene name Pr-deGFP-MGapt, Addgene plasmid #67734) for protein and mRNA measurement, and pIVEX-pT7-GFP-MG (Addgene name PT7-deGFP-MGapt, Addgene plasmid #67741) for mRNA preparation. These plasmids are described in (9). More information on these and links to their sequence and other info are given in the Supplementary Table S1. Plasmids were a kind gift from Dr. Murray's lab. BL21-Rosetta 2 strain for making crude extract was obtained from Novagen. Plasmid DNAs used for measuring protein and mRNA production were prepared using Qiagen Plasmid Midi prep kits.

2.4 mRNA preparation

First polymerase chain reaction (PCR) was performed on pIVEX2.3 PT7-deGFP-MGapt plasmid using T7 promoter and T7 terminator primers obtained from IDT. The linear PCR was used as starting material for setting up TX reactions using T7 RNA polymerase (Cellscript).

3. Results and discussion

We begin by examining the time-dependent gene expression profiles for increasing NTP concentrations. We use a plasmid described in Siegal-Gaskins *et al.* (9) with a built-in RNA aptamer (35-bp MGapt sequence), which contains a binding pocket for MG dye and a fluorescent protein for accomplishing the simultaneous measurement of mRNA and protein. The result of a typical experiment is shown in Figure 1.

Figure 1 shows the time evolution of protein production as measured by GFP fluorescence for various NTP concentrations. We illustrate only the initial 8 h of the experiment, prior to
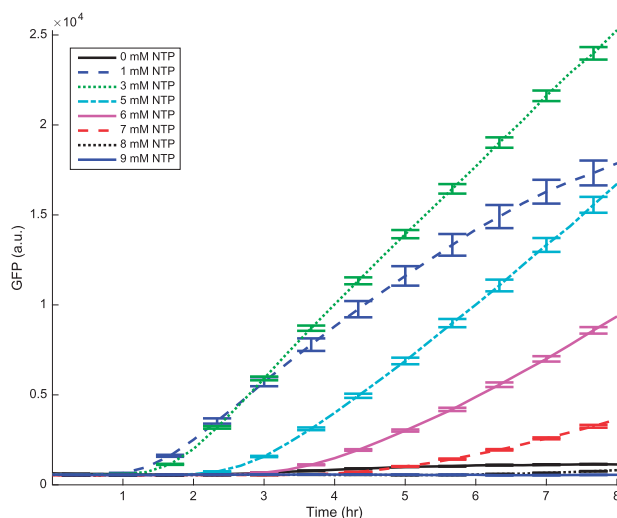

Figure 1. Translation kinetics demonstrating the GFP protein production for various NTP concentrations with DNA as the starting material. Data are measured every 20 min, while error bars, denoting the standard error of the mean, are plotted for every other data point for clarity. Mean and standard error are calculated over six replicates. Concentrations of Mg^{2+} and K^+ are 18 mM and 91 mM, respectively.

saturation. Notice that protein production at early times is suppressed by increasing the amounts of NTP. This observation conflicts with the hypothesis that resource limitation is driven by high transcriptional activity causing lower protein production. However, to further understand the roles of TX and of TL, we proceeded to perform the experiments with the process of TX eliminated. We describe these experiments subsequently.

We purified the mRNA from the plasmid mentioned earlier. Similar to the TX and TL process described previously, we measured the protein expression from purified mRNA added to the reaction mixture, in the absence of DNA. Therefore, in this experiment, the only processes affecting gene expression are mRNA decay and the time-dependent translation rate. The MG binding 35-bp aptamer allows us to measure the mRNA levels, whereas GFP fluorescence gives us access to protein abundance. The resulting mRNA and protein profiles are shown in Figures 2 and 3, respectively. Messenger RNA profiles in Figure 2 show approximate exponential decay, as expected.

Using both the mRNA and protein profiles, we extract time-dependent TL rates, following methods similar to those appearing in Siegal-Gaskins *et al.* (9) from 2014. We assume that GFP (g) and MG (m) are related to protein (p) and mRNA (r) expression as follows:

$$g(p) = \alpha p + g_0, \tag{1}$$

$$m(r) = \beta r + m_0. \tag{2}$$

Here g_0, m_0 are parameters accounting for autofluorescence and, in general, vary between experiments, whereas α, β are proportionality constants that convert between fluorescence measurements and the corresponding protein or mRNA concentrations. Importantly, we assume that α and β are fixed constants, independent of the experiment under consideration. Note that since mRNA is unstable and undergoing approximate exponential decay (see Figure 2), we can estimate m_0 as the final temporal measurement of m for each experiment.

The fundamental quantity of interest is the (generally) time-varying TL rate $k_p(t)$. Since only TL is occurring, we assume that the rate of protein production is directly proportional to the amount of mRNA $r(t)$ at time t:
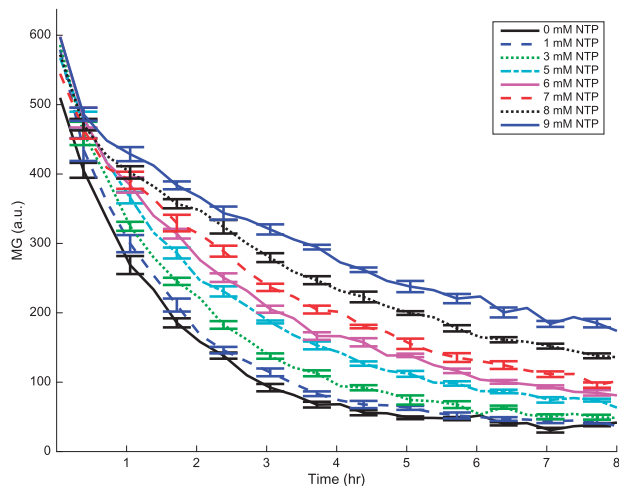
$$\frac{dp}{dt}(t) = k_p(t)r(t), \tag{3}$$

To estimate $k_p(t)$, we must first relate it to the observed quantities g and m. Defining

$$M(t) := \int_0^t (m(s) - m_0)\, ds, \tag{4}$$

$$G(M) := g(p(M)), \tag{5}$$

where $p(M)$ is the protein concentration as a function of M, one can show (for details, including justification that $p = p(M)$ is well defined, see Appendix) that $G(M)$ satisfies the following ordinary differential equation (ODE):

$$\frac{dG}{dM}(M(t)) = \frac{\alpha}{\beta} k_p(t). \tag{6}$$

Since α and β are constants across experiments, equation (6) implies that dG/dM can be used as a proxy for the TL rate k_p. Thus, to analyze the qualitative effects of Mg^{2+} and NTP on TL, we compute slopes in the G-M plane. See Figure 4 for a sample calculation, which we describe in the following.

We also note that the quantity $M(t)$ had been defined in a previous study (9) and can be interpreted as proportional to the amount of protein produced, assuming a constant TL rate [see the definition in equation (4)]. Thus, plotting G against M, we obtain a measure of the instantaneous TL rate.

To calculate the translation rate (technically $\frac{\alpha}{\beta} k_p$) for each experiment, we observe the following general phenomenon. For all replicates, we observe a lag time t_0 (see, e.g. Figure 1 or 3), where protein levels appear to be approximately constant. Assuming this signal is generated by autofluorescence (background emission from other biomolecules) and thus is not due to production of the GFP-tagged protein of our interest, TL is yet to start in earnest. This is verified in the G-M plane as in Figure 4, where a slope of approximately zero is observed initially. Afterwards, there exists a regime where translation occurs at a constant rate, which can be taken as proportional to $k_p(t)$ via equation (6). Toward the end of each experiment, protein level
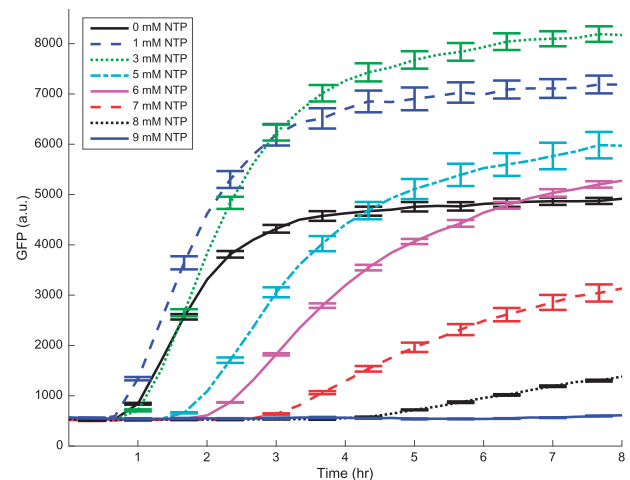

Figure 2. RNA decay profile for various NTP concentrations as a function of time, with mRNA as the starting material. Data are measured every 20 min, while error bars, denoting the standard error of the mean, are plotted for every other data point. Mean and standard error are calculated over six replicates. Concentrations of Mg^{2+} and K^+ are 18 mM and 91 mM, respectively.

Figure 3. Translation kinetics showing the GFP protein production for various NTP concentrations with mRNA as the starting material. Data are measured every 20 min, while error bars, denoting the standard error of the mean, are plotted for every other data point. Mean and standard error are calculated over six replicates. Concentrations of Mg^{2+} and K^+ are 18 mM and 91 mM, respectively.
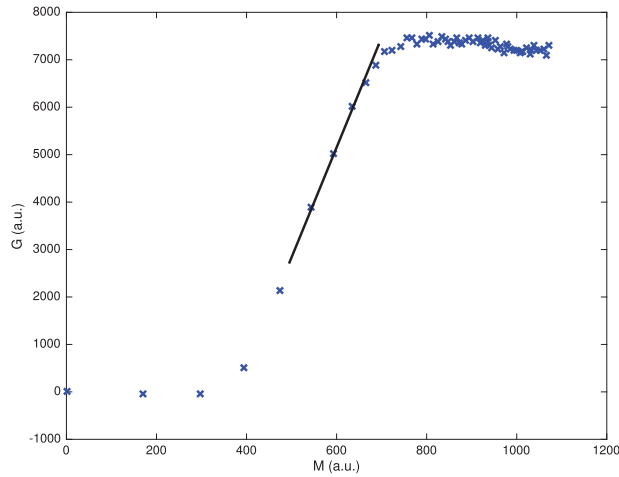
Figure 4. The change in protein versus the integral of the mRNA profile at 21 mM Mg^{2+} and no additional NTP. For most replicates and Mg^{2+}/NTP concentrations, we observe a clear region of nearly constant translation rate. The extracted rate (i.e. slope) for this experiment is shown via the black solid line.

Figure 5. Surface plot showing the translation rate as a function of various NTP and Mg^{2+} concentrations.

saturates and again the slope of $G(M)$ approaches zero. The initial TL rate is thus taken, in this work, as the slope of $G(M)$ in the region of approximate linear growth. This behavior, taken together with that of the early and late regimes, implies that the slope should be largest during the period of linear growth, although some exceptions exist due to noise and the difficulty in computing derivatives with discrete data. To that end, we exclude early and late data from TL rate extraction, where these effects are most noticeable. The basis for our algorithm for computing k_p is then the following: transform to the (M, G) plane, compute moving windows of fixed length (five data points were used, but the results are robust to this value), use a least-squares regression to fit a line to the data and measure the translation rate k_p as the maximum value over all such moving windows.

To verify that TL occurs, at least on an intermediate time window, at an approximately constant rate, we plot the GFP-MG (i.e. protein-RNA) translation data in the (G, M) plane for each experiment (each NTP and Mg^{2+} is performed with six replicates). For a demonstrative example, see the plot in Figure 4; all 384 experiments are similar. Blue crosses represent experimental data points. In each case, we observe rapid linear growth between regions of slower growth; the initial slow growth corresponds to the experimental delay, which implies approximately no change in protein production: $dG/dM = 0$, while the latter to the diminished mRNA concentration in the well (i.e. saturation). This approximately linear regime is where we measure the translation rate k_p via a least-squares regression (slope of black line). Note that the clustering of data points for large M values is due to the fact that the transformation $t \to M(t)$ is not an isometry. As time t increases, the decay of mRNA (Figure 2) implies that the total amount of mRNA (measured via M) stabilizes.

Before describing the results, we offer a brief discussion of the initial lag and its impact on our analysis. We believe it arises from an initial formation of molecules necessary for processes such as translation, as well as system calibration to initial mixing and temperature change. We expect our fluorescence measurements to be linear in the number of molecules, on average, in the low signal limit, so we do not anticipate a delay originating from the sensitivity limit of the optical measurement. Also, we have noticed that this delay varies slightly for runs on different days with different samples. If the reactions were reliable
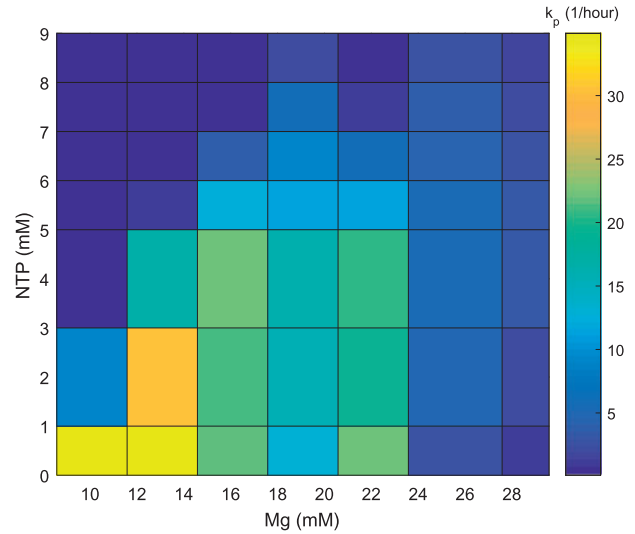
and it was only due to machine sensitivity, we would have expected the delays to be consistent.

We argue that our conclusions are robust to this phenomenon. Since our analysis only depends on changes in protein levels, our extracted TL rates from the intermediate time range do not depend on the early-phase dynamics. Thus, even if we allow for the possibility that the lag has to do with a sensitivity limit to small protein amounts, our results arise from differences in strong fluorescence signals associated with detectable protein levels. Also, in our major experiments, where the initial material is mRNA, the lag times are typically smaller than the analogous experiments with DNA as initial material, for comparable levels of NTP and Mg^{2+}.

The computed translation rate is plotted against both NTP and Mg^{2+} concentrations in Figure 5, confirming our hypothesis that additional NTP is directly inhibiting translation.

Analyzing Figure 5, we observe a complex interdependence between Mg^{2+} and NTP concentrations on the TL rate dynamics. Specifically, for each value of NTP, two distinct maxima exist as a function of Mg^{2+}. As the NTP concentration increases, one of these maxima shifts to increasing values of Mg^{2+}. Recalling that NTP-Mg^{2+} is the biologically relevant complex, we have developed a phenomenological model to explain this maxima shifting. For the discussion of multiple maxima, see below.

In this model, a greater amount of NTP requires a greater amount of Mg^{2+} to be functional. Otherwise, the free NTP, unbound to Mg^{2+}, 'poisons' the TL system. Initially, this may appear unintuitive in our experimental system, because the total concentration of NTP (a few mMs) is two to three times smaller than the total Mg^{2+} concentrations, with dissociation constant on the order of 0.01 mM (12). However, we recall that TL is affected not by the total ion concentration but instead by the free ions in the solution. Nierhaus (13) have shown the binding of ribosomes to a significant fraction of Mg^{2+} and K^+, thereby leaving very little cytosolic ions available.

Let us consider the competition for Mg^{2+} between NTP and other species, such as ribosomes, with binding sites for the ion. Assume that the competitors of NTP have the same Mg^{2+} binding affinity K_O. We can now consider two extreme regimes, which relate the values of K_O with a typical Mg^{2+} binding affinity of an NTP, K_{NTP}. If $K_O \ll K_{NTP}$, then Mg^{2+} will first bind to the

competitors and only the remaining ions would be available for binding to NTP. For the concentrations considered in this work, this condition is equivalent to the total concentration of Mg^{2+} available to NTP being reduced by a fixed amount. Conversely, $K_O \gg K_{NTP}$ leads to a fixed fraction of non-NTP bound Mg^{2+} to be free, the remainder being bound to competitors. In the first scenario, added NTP requires almost equal increase in concentration of Mg^{2+} for partial reversal of TL suppression, a stoichiometric requirement. In the second case, one needs to add more Mg^{2+} to observe the same effect, since unbound sites from the weak competitors would bind to some of the additional Mg^{2+}. Examining our data, the ratio of added Mg^{2+} to added NTP, for TL rescue, seems to be approximately 1:1. Also the NTP-Mg^{2+} compensation seems to be occurring for additional Mg^{2+} about a certain amount, approximately 10 mM. These observations provide evidence for the first scenario; specifically that approximately 10 mM of Mg^{2+} is strongly bound to competitor molecules. The concentration of Mg^{2+} available for binding with NTP to form NTP-Mg^{2+} complex, which is central to gene expression (14), is therefore treated as an available total concentration in our mathematical model. In other words, available magnesium $[Mg^{2+}]_{Avail}$ is the difference of total and bound (sequestered) magnesium, $[Mg^{2+}]_T$ and $[Mg^{2+}]_{Bound}$, respectively:

$$[Mg^{2+}]_{Avail} = [Mg^{2+}]_T - [Mg^{2+}]_{Bound}.$$

The above observation suggests that $[Mg^{2+}]_{Bound}$ is approximately constant, which we now assume for the remainder of the work.

More precisely, we assume that the translation rate takes the following general form:

$$k_p = a \cdot \frac{[NTP\text{-}Mg^{2+}]}{[NTP\text{-}Mg^{2+}] + b[NTP] + c} \cdot \frac{1}{1 + [Mg^{2+}]_{Avail}} \quad (7)$$

Here $[NTP\text{-}Mg^{2+}]$ denotes the concentration of the NTP-Mg^{2+} complex and is the driver of translation. The above expression represents the competition at the binding site between the unbound NTP and NTP-Mg^{2+} molecules, with b and c denoting (relative) inverse dissociation constants and a the maximum possible TL rate. We also have included a completely phenomenological Mg^{2+}-dependent suppression of the form $1/(1 + [Mg^{2+}]_{Avail})$, since it is known that Mg^{2+} in abundance will inhibit TL (15–17).

To calculate the concentrations used in the above formula, we assume all reactions are in equilibrium, and thus concentrations can be calculated via a steady-state analysis. We have the following association–dissociation reaction between Mg^{2+} and NTP:

$$Mg^{2+} + NTP \underset{k_{-1}}{\overset{k_1}{\rightleftharpoons}} NTP\text{-}Mg^{2+},$$
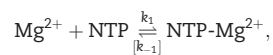
from which we can calculate the concentration of [NTP-Mg^{2+}] as a function of total concentrations $[Mg^{2+}]_T$, $[NTP]_T$ $(= [NTP] + [NTP\text{-}Mg^{2+}])$ and the dissociation constant $K_d (= k_{-1}/k_1)$. In general, we can show that for each total concentration of NTP, the above will possess a unique relative maximum in $[Mg^{2+}]_T$, which increases as the total amount of NTP is increased. A sample plot is included in Figure 6 for demonstrative purposes.

The previous model does not capture the two-peak structure of the data sets. We believe that there are two distinct
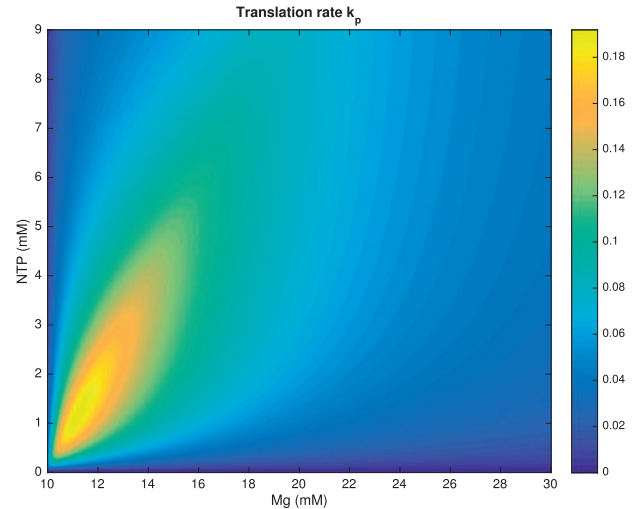

Figure 6. Heat map showing the translation rate as a function of total NTP and total Mg^{2+} concentrations for the one maximum model (7). $[Mg^{2+}]_{Bound}$ is assumed to be 10 mM.

influences of Mg^{2+} on TL. One of these has to do with NTP titration, as described previously. The other involves the stabilization of RNA and other molecules involved in translation (13,18) and that effect has an optimal concentration requirement. The superposition of two such effects could then lead to two local maxima. Disentangling these two effects from the experimental data is indeed an interesting question.

Several processes that did not get explicitly modeled are worth considering more explicitly in future work. Aminoacyltransfer RNA synthetases (aaRS's) rely on both ATP and Mg^{2+} to function, which could give rise to complex NTP and Mg^{2+} dependencies in gene expression. Furthermore, different synthetases seem to require a varying number of Mg^{2+} ions for each ATP (19). At present, we do not understand the 1:1 compensation effect in that framework, and further detailed studies of quantitative models including aminoacylation effects [see (20)] are needed.

Another possible mechanism of NTP-dependent suppression of TL is that accumulated inorganic phosphate depletes Mg^{2+} levels and leads to reduced ribosome activity through 16 S rRNA cleavage in *E. coli* cell-free (21,22). This mechanism indeed has the same qualitative effect of removal of free Mg^{2+} leading to inhibited TL. However, in the experiments of Failmezger *et al.* (22), 16S rRNA degrades steadily with the timescale of hours. If this was the main effect in our experimental conditions, we would have expected to observe a steady decrease in translation rate. Since we instead measure translation occurring at a nearly constant rate over a time span of several hours, we are not confident this mechanism explains the main observation in our data.

Basic cellular processes like TX and TL require many resources. As we try to build synthetic gene regulation networks, we need to understand competition for resources giving rise to limitations and trade-offs. Both mathematical modeling and experimental studies are directed toward elucidation of this issue (23,24,9). In the system studied, we provide evidence that suppression of gene expression due to added NTP is not primarily due to competition between TX and TL as has been proposed in (9), but we suggest that the limitation of available free Mg^{2+} plays a role in this suppression. This suggestion is based on the observation that the suppression due to additional NTP is partly

relieved by adding more Mg^{2+}. In general, because of the nontrivial interaction between different resources, more studies need to be done scanning multiple parameters simultaneously, while monitoring a particular phenotype.

Finally, the fine-tuning needed in the TX-TL raises questions regarding the optimization of gene expression *in vivo*. Our knowledge of sensing and controlling levels of crucial reagents in the cell is currently incomplete at best, although quite a bit is known about homeostasis of ATP levels (25). These synthetic biology studies therefore provide an important impetus for furthering our understanding.

Supplementary data

Supplementary Data are available at SYNBIO Online.

References

1. Shimizu,Y., Inoue,A., Tomari,Y., Suzuki,T., Yokogawa,T., Nishikawa,K. and Ueda,T. (2001) Cell-free translation reconstituted with purified components. *Nat Biotechnol*, 19, 751.
2. Noireaux,V., Bar-Ziv,R. and Libchaber,A. (2003) Principles of cell-free genetic circuit assembly. *Proc Natl Acad Sci U S A*, 100, 12672–12677.
3. —— and Libchaber,A. (2004) A vesicle bioreactor as a step toward an artificial cell assembly. *Proc Natl Acad Sci U S A*, 101, 17669–17674.
4. ——, Maeda,Y.T. and Libchaber,A. (2011) Development of an artificial cell, from self-organization to computation and self-reproduction. *Proc Natl Acad Sci U S A*, 108, 3473–3480.
5. Shin,J. and Noireaux,V. (2012) An *e. coli* cell-free expression toolbox: application to synthetic gene circuits and artificial cells. *ACS Synth Biol*, 1, 29–41.
6. Sun,Z.Z., Hayes,C., Shin,A., Caschera,J.F., Murray,R.M. and Noireaux,V. (2013) Protocols for implementing an *escherichia coli* based TX-TL cell-free expression system for synthetic biology. *J Vis Exp*, 79, e50762.
7. Kuruma,Y. and Ueda,T. (2015) The pure system for the cell-free synthesis of membrane proteins. *Nat Protoc*, 10, 1328.
8. Biotechnology: cell-free biotech will make better products. The Economist, May 6, 2017.
9. Siegal-Gaskins,D., Tuza,Z.A., Kim,J., Noireaux,V. and Murray,R.M. (2014) Gene circuit performance characterization and resource usage in a cell-free "breadboard". *ACS Synth Biol*, 3, 416–425.
10. Caschera,F. and Noireaux,V. (2014) Synthesis of 2.3 mg/ml of protein with an all *escherichia coli* cell-free transcription-translation system. *Biochimie*, 99, 162–168.
11. —— and —— (2015) Preparation of amino acid mixtures for cell-free expression systems. *Biotechniques*, 58, 40–43.
12. Rose,I.A. (1968) The state of Magnesium in cells as estimated from the adenylate kinase equilibrium. *Proc Natl Acad Sci USA*, 61, 1079–1086.
13. Nierhaus,K.H. (2014) Mg^{2+}, K^+, and the ribosome. *J Bacteriol*, 196, 3817–3819.
14. Wolf,F.I. and Cittadini,A. (2003) Chemistry and biochemistry of Magnesium. *Mol Aspects Med*, 24, 3–9.
15. Zagǒrski,W., Filipowicz,W., Wodnar,A., Leonowicz,A., Zagǒrska,L. and Szafranski,P. (1972) The effect of Magnesium-ion concentration on the translation of phage-f2 RNA in a cell-free system of *escherichia coli*. *Eur J Biochem*, 25, 315–322.
16. Brandi,L., Fabbretti,A., La Teana,A., Abbondi,M., Losi,D., Donadio,S. and Gualerzi,C.O. (2006) Specific, efficient, and selective inhibition of prokaryotic translation initiation by a novel peptide antibiotic. *Proc Natl Acad Sci USA*, 103, 39–44.
17. Lancaster,A.M., Jan,E. and Sarnow,P. (2006) Initiation factor-independent translation mediated by the hepatitis C virus internal ribosome entry site. *RNA*, 12, 894–902.
18. Lightfoot,D.A. (1988) Magnesium-dependence of *in vitro* translation programmed by gene-specific mRNAs. *Nucleic Acids Res*, 16, 4164.
19. Airas,R.K. (1996) Differences in the Magnesium dependences of the class I and class II aminoacyl-trna synthetases from *escherichia coli*. *FEBS J*, 240, 223–231.
20. MatsuuraTanimura,T., Hosoda,N. and Yomo,K.T., (2017) Reaction dynamics analysis of a reconstituted *escherichia coli* protein translation system by computational modeling. *Proc Natl Acad Sci U S A*, 114, E1336–E1344.
21. Kim,T.-W., Kim,D-M. and Choi,C-Y. (2006) Rapid production of milligram quantities of proteins in a batch cell-free protein synthesis system. *J Biotechnol*, 124, 373–380.
22. Failmezger,J., Nitschel,R., Sánchez-Kopper,A., Kraml,M., Siemann-Herzberg,M. and Wieden,H.-J. (2016) Site-specific cleavage of ribosomal RNA in *escherichia coli*-based cell-free protein synthesis systems. *PLoS One*, 11, e0168764.
23. Borkowski,O., Ceroni,F., Stan,G.B. and Ellis,T. (2016) Overloaded and stressed: whole-cell considerations for bacterial synthetic biology. *Curr Opin Microbiol*, 33, 123–130.
24. Gyorgy,A. and Del Vecchio,D. Limitations and trade-offs in gene expression due to competition for shared cellular resources. In: *IEEE 53rd Annual Conference on Decision and Control (CDC), 2014*. IEEE, Los Angeles, CA, USA. P. 5431–5436.
25. Hara,K.Y. and Kondo,A. (2015) ATP regulation in bioproduction. *Microb Cell Fact*, 14, 198.

Appendix

In this section, we formally derive equation (6). Assume that the mRNA concentration $r(t) > 0$ for all t in each experiment and that translation can be described by (3):

$$\frac{dp}{dt}(t) = k_p(t)r(t).$$

Equations (2) and (4) imply that

$$M(t) = \beta \int_0^t r(s) \, ds,$$

so that $M'(t) = r(t) > 0$, i.e. M is an increasing function of t. Thus, $M(t)$ is invertible, and we can solve

$$t = t(M)$$

on some interval $M \in [0, M_{max})$. Note that $M_{max} < \infty$ as $r(t)$ is exponentially decreasing, although this is not strictly necessary. Furthermore, we can compute the derivative of this function via the inverse function theorem:

$$\frac{dt}{dM} = \frac{1}{M'(t(M))} = \frac{1}{\beta r(t(M))}. \tag{8}$$

Defining the GFP marker as a function of M,

$$G(M) := g(p(t(M))),$$

is thus well-defined, and we can compute its derivative using the chain rule:

$$\frac{dG}{dM} = \frac{dg}{dp}(p(t(M)))\frac{dp}{dt}(t(M))\frac{dt}{dM}(M).$$

Equation (1) implies that $\frac{dg}{dt} = \alpha$, equation (3) that $\frac{dp}{dt} = k_p(t(M))r(t(M))$, and equation (8) provides the last term on the right-hand side. Canceling $r(t(M))$ yields the expression

$$\frac{dG}{dM}(M) = \frac{\alpha}{\beta}k_p(t(M)),$$

which is precisely (6), as desired.